Available online at www.sciencedirect.com
SCIENCE DIRECT
Journal of Power Sources 146 (2005) 478–481
JOURNAL OF POWER SOURCES
www.elsevier.com/locate/jpowsour

Study of Li insertion mechanisms in transition metal antimony compounds as negative electrodes for Li-ion battery

Costana Mihaela Ionica, Pierre Emmanuel Lippens, Josette Olivier Fourcade, Jean-Claude Jumas *

Laboratoire des Agrégats Moléculaires et Matériaux Inorganiques (CNRS UMR 5072), Université Montpellier II, CC 015, Place E. Bataillon, 34095 Montpellier Cedex 5, France

Available online 28 April 2005

Abstract

MSb (M = Ni, Co, Fe, Mn) alloys with a NiAs type structure were synthesized by ceramic route and evaluate as a negative electrode material for rechargeable lithium batteries. Electrochemical tests demonstrated that initial charge and discharge capacities of this materials were ca. 390 and 330 mAh g^{-1}, respectively. Ex situ XRD of MnSb electrodes showed that LiMnSb and Li_3Sb were successively formed during lithium insertion. The ^{121}Sb Mössbauer spectra show that the insertion mechanism during discharge involves the formation of several lithium-containing compounds such as LiMnSb, Li_3Sb with manganese extrusion. During the subsequent charge a more complex mechanism occurs involving MnSb, modified LiMnSb alloy and metallic Sb formation.

Keywords: Alloys materials; Lithium insertion mechanism; ^{121}Sb Mössbauer spectroscopy

1. Introduction

The development of new electrode materials for Li-ion batteries has important commercial implications. The electrochemical performances of carbon negative electrodes improve continuously, reversible capacities greater than 372 mAh g^{-1} (for the charged LiC_6) have been reached [1–3]. The main disadvantage of graphite is the low discharge rate capability limiting in a wild field of applications. For this reason, together with safety problems and the demand of high-energy storage batteries, it is necessary to find carbon alternatives. Lithium alloys systems Li_xM (M = Al, Sb, Si, Sn) have been extensively studied by Besenhard and Huggins [4–6]. Cyclic performance of these alloys deteriorates due of a large Li-driven volume variation, which causes mechanical disintegration and a loss of electrical contact between the particles. There was a great interest for intermetallic materials, in which active component to lithium is dispersed in the inactive one. In these compounds, the active element reacts with lithium to form lithium alloy while the inactive material plays the role of a matrix buffering the volume expansion. The antimony–metal transition systems were intensively studied as intermetallic electrodes [7–9]. We are interested in MSb intermetallic alloys with nickel arsenide type structure, where M is a transition metal (Ni, Co, Fe, Mn). The NiAs ($B8_1$) structure has the hexagonal unit cell. The Sb is surrounded by six M atoms at the apices of a right-trigonal prism, while the coordination about M is six Sb atoms in a distorted octahedral array, with two additional M neighbours along the *c*-axis [10]. These compounds are well known to exhibit a variety of physical properties [11]. For example, MnSb is ferromagnetic with a transition temperature T_C = 600 K, CrSb is antiferromagnetic, T_N = 400 °C, and CoSb is paramagnetic [12]. The lithium insertion in these alloys takes often place through multi-phase mechanisms and the X-ray diffraction patterns of the discharged electrodes do not show well-defined peaks. The use of an alternative technique such as Mössbauer spectrometry is indispensable to investigate the electrochemical reactions of the anode at atomic scale. In this paper we report the electrochemical properties of these materials and we focus on MnSb for study of lithium insertion mechanisms.

* Corresponding author.
E-mail address: jumas@univ-montp2.fr (J.-C. Jumas).

0378-7753/$ – see front matter © 2005 Elsevier B.V. All rights reserved.
doi:10.1016/j.jpowsour.2005.03.054

2. Experimental aspects

The alloy samples were prepared by heating weighed quantities of the components in evacuated and sealed silica tubes at temperatures between 700 and 1200 °C for about 20 h and finally the tubes samples were slowly cooled in the furnace to room temperature. In order to obtain single phase intermetallic compounds, the alloys were annealed at appropriate temperature.

To identify the phases of alloy samples, X-ray diffraction (PHILIPS XPert MPD) was carried out using Cu Kα radiation in continuous mode. The powdered samples were observed by scanning electron microscopy (SEM) in order to characterize both the sample morphology and the particle size. The particle size distribution was measured with MALVERN Instruments laser diffraction particle analyser, in which the suspensions were treated with ultrasound before and during the measurement to break larger aggregates in suspension down to smaller ones.

Electrodes containing 82 wt.% sample, PTFE binder 12 wt.% and carbon black were pressed in 7 mm diameter pellets. The electrochemical properties of the materials were measured with Li|1 M $LiPF_6$ (PC:EC:DMC = 1:1:3, v/v)|MSb cells using a Mac Pile II system at *C*/20 rate for both charge and discharge, between 0.05 and 1.2 V versus Li^+/Li. The MnSb cells were cycled between 0.2 and 1.4 V. To clarify the electrode reaction mechanism, XRD were carried out for MnSb electrodes by stopping lithium insertion/extraction at various voltages.

^{121}Sb Mössbauer measurements were performed using a ^{121m}Sn in $BaSnO_3$ source of nominal activity 0.5 mCi on an EG & G constant acceleration spectrometer in transmission mode. During the measurements, both source and absorbers were simultaneously cooled down to 4 K in order to increase the fraction of recoil-free absorption and emission processes. Measurements were performed at several depths of discharge and charge. The cells were opened inside the glove box and the electrode materials containing the active material were placed on specific sample holder transparent for the γ rays.

3. Results and discussions

The samples were identified like single phase compounds. The refinement of the unit cell parameters leads to hexagonal structures: NiSb with $a = 3.94$ Å and $c = 5.14$ Å, CoSb with $a = 3.89$ Å and $c = 5.19$ Å, FeSb with $a = 4.11$ Å and $c = 5.16$ Å in good agreement with published data [13–17]. The lattice constants of the MnSb sample ($a = 4.19$ Å and $c = 5.74$ Å) are close to those for the $Mn_{1.09}Sb$ composition ($a = 4.17$ Å and $c = 5.75$ Å) [18,19]. SEM and laser diffraction images of the sample powders were used to estimate the particle size, which was ranged 1–25 μm.

Fig. 1 illustrates charge–discharge curves of CoSb and MnSb samples. The first discharge capacity is ca. 550 mAh $g^{-1}$and the reversible gravimetric capacity in

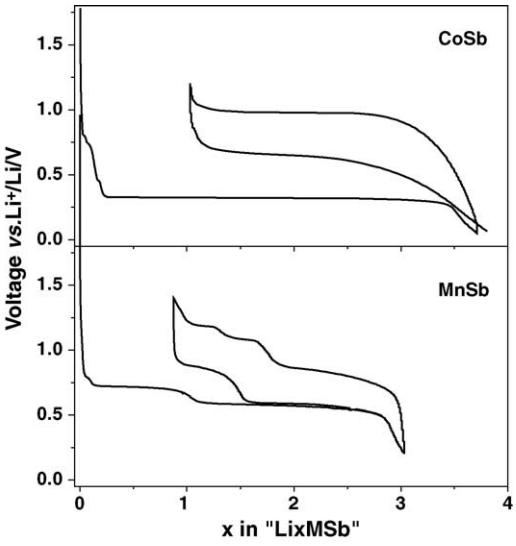

Fig. 1. Discharge–charge curves of CoSb and MnSb electrode materials.

the first cycle is 398 mAh g^{-1}, suggesting that CoSb has a large power density as anode material for lithium-ion batteries. It is noteworthy that considering the density of CoSb ($\rho = 8.88$ g cm^{-3}) the volumetric capacity is 3534 mAh cm^{-3}, which is much larger than that of the graphite electrode of ca. 800 mAh cm^{-3}. The discharge potential for the CoSb electrode drops rapidly to 0.8 V versus Li. This process is associated with the formation of a SEI (solid electrolyte interface) passivating film as a result of the reduction reactions of Li with electrolyte onto the carbon particles [8]. The passivating film is mainly composed of Li_2CO_3 and $ROCO_2Li$ [20]. The first discharge proceeds through a voltage plateau corresponding to a two-phase reaction, whose potential 0.32 V is lower than for metallic Sb (0.9 V) [21]. The end of the plateau corresponds to the insertion of 3.3 Li, while additional 0.4 Li are required for a discharge at 0.05 V. Assuming the simple electrochemical reaction with transformation $CoSb/Li_3Sb$ during discharge

$$3Li^+ + 3e^- + CoSb \rightarrow Li_3Sb + Co$$

the volume expansion of the electrode material in the fully lithiated sample is 143%. Such a reaction has been confirmed by Mössbauer measurements at low lithium rate [22] and first-principles calculations [23]. The NiSb and FeSb alloys present the same discharge profiles with a voltage plateau at 0.35 and 0.39 V, respectively.

For MnSb the potential first drops to 0.8 V, then a plateau at 0.78 V corresponding to a two-phase reaction is observed. The end of this plateau corresponds to the insertion of approximately 1.1 Li. The following step in the discharge process is reached by the plateau at 0.55 V up to about 2.8 Li and the discharge at 0.2 V is obtained for 3 Li. The volumetric reversible capacity of 2253 mAh cm^{-3} was determined for MnSb electrode.

To check phase changes during the electrochemical lithiation XRD was carried out on the samples obtained at various

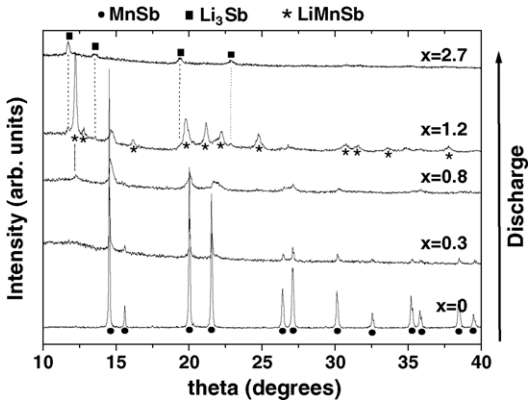

Fig. 2. XRD spectra of MnSb while discharge at 0.2 V.

Li-insertion steps (Figs. 2 and 3). The XRD graph of the starting electrode shows the peaks characteristics of MnSb. While discharge at 0.7 V ($x = 0.8$ Li) the decrease in the intensity of the MnSb peaks and the increase of another peak around 12.25° were observed. At the end of the first plateau ($x = 1.2$ Li), MnSb has been transformed into LiMnSb (fluorite-type structure) and Li_3Sb. The contribution of the main peak (1 0 1) of MnSb is found at ca. 14.64°. At the end of the second plateau ($x = 2.8$ Li) Li_3Sb is confirmed as a new phase from the XRD peak analysis. During the charge process the Li_3Sb phase is found to disappear and the LiMnSb phase is restructured (Fig. 3). At the end of the charge ($x = 0.7$) MnSb is regenerated.

Both XRD and galvanostatic measurements suggest that electrochemical reactions in MnSb electrodes during the insertion process could be written as

$$\mathrm{MnSb} + \mathrm{Li^+} + \mathrm{e^-} \rightarrow \mathrm{LiMnSb} + \mathrm{Mn}$$

$$\mathrm{LiMnSb} + 2\mathrm{Li^+} + 2\mathrm{e^-} \rightarrow \mathrm{Li_3Sb} + \mathrm{Mn}$$

The ^{121}Sb Mössbauer spectra of MnSb samples were registered at different depths of discharge (Fig. 4) and charge (Fig. 5).

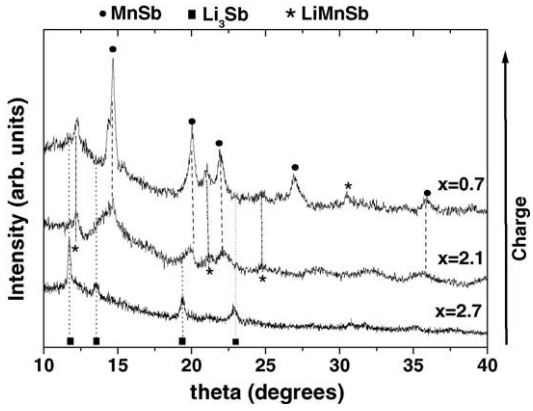

Fig. 3. XRD spectra of MnSb while charge at 1.4 V.

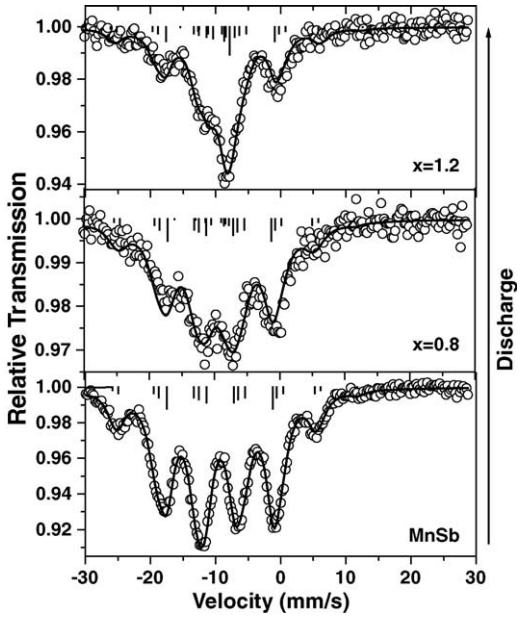

Fig. 4. ^{121}Sb Mössbauer spectra of MnSb while discharge.

The Mössbauer absorption of ^{121}Sb in MnSb shows a strong magnetic hyperfine field and a small quadrupole interaction at the Sb sites. The spectrum of the starting electrode shows four broadened peaks each containing three unresolved lines and two small satellites each containing two unresolved lines. The corresponding refined hyperfine parameters are reported in Table 1. While discharge at 0.6 V the Mössbauer spectra show the apparition of two new components attributed to the formation of the LiMnSb ($\delta \sim -1.14\,\mathrm{mm\,s^{-1}}$) and Li_3Sb ($\delta_1 \sim 0.9\,\mathrm{mm\,s^{-1}}$), with the decrease of the MnSb contribution. At the end of the first

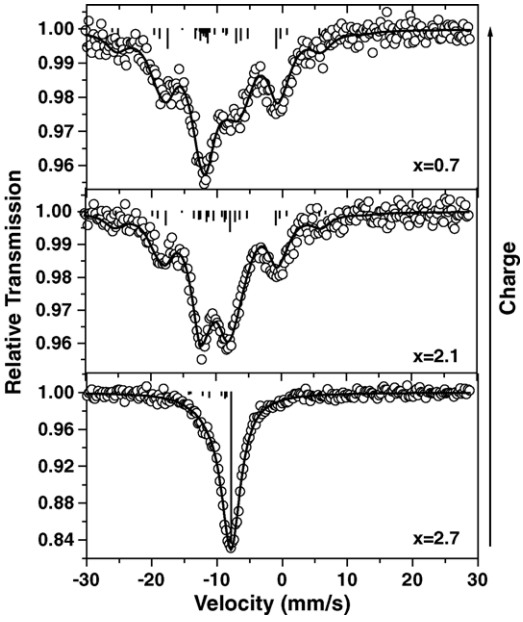

Fig. 5. ^{121}Sb Mössbauer spectra of MnSb while charge.

Table 1
^{121}Sb Mössbauer parameters obtained from experimental data

Sample (MnSb)	δ (mm s^{-1})	Δ (mm s^{-1})	Γ (mm s^{-1})	H_{hf} (T)	C (%)
x = 0.8 (0.7 V)	−0.78 (3)	1.88 (8)	1.21 (8)	37.8	–
	−0.68 (0)	1.91 (0)	1.89 (0)	37.0	85
	−1.18 (0)	15.84 (0)	1.89 (0)	–	12
	0.94 (0)	–	1.89 (0)	–	3
x = 1.2 (0.6 V)	−0.69 (0)	1.58 (0)	1.08 (1)	38.8	58
	−1.13 (5)	14.27 (1)	1.08 (1)	–	28
	0.89 (0)	–	1.08 (1)	–	14
x = 2.7 (0.4 V)	0.90 (7)	–	1.81 (2)	–	88
	−1.70 (9)	19.22 (1)	1.81 (2)	–	12
x = 2.1 (1 V)	−0.69 (0)	1.68 (0)	1.52 (8)	39.1	55
	−1.13 (0)	13.64 (0)	1.52 (8)	–	20
	−3.68 (0)	0.2 (1)	1.23 (0)	–	12
	0.89 (0)	–	1.89 (0)	–	13
x = 0.7 (1.4 V)	−0.68 (0)	1.61 (0)	1.93 (3)	38.7	75
	−1.11 (0)	14.0 (9)	1.93 (3)	–	10
	−3.27 (5)	2.93 (0)	1.93 (3)	–	15

δ: isomer shift relative to $Ba^{121m}SnO_3$ source, Δ: quadrupole coupling, H_{hf}: magnetic hyperfine field, Γ: linewidth, C: relative contribution.

discharge the Mössbauer spectrum (which correspond with the beginning of the charge, Fig. 5) mainly reflects Li_3Sb ($\delta_1 \sim 0.9$ mm s^{-1}) although there is a small contribution assigned to highly dispersed electrochemical, poor in antimony Li_xMnSb_y ($\delta_2 \sim -1.7$ mm s^{-1}). On charge the mechanism is more complex. For the sample charged at 1 V (x = 2.1 Li) the experimental data were fitted with four different environments for Sb. Three phases were identified that have been attributed to MnSb with magnetic hyperfine field of 39.1 T ($\delta_1 \sim -0.69$ mm s^{-1}), LiMnSb ($\delta_2 \sim -1.13$ (7) mm s^{-1}), Li_3Sb ($\delta_4 \sim 0.89$ mm s^{-1}). On full charge at 1.4 V (x = 0.7 Li) the Mössbauer spectrum shows the presence of MnSb, LiMnSb alloy and metallic Sb ($\delta_3 \sim -3.27$ mm s^{-1}, Δ_3 = 2.93 mm s^{-1}).

4. Conclusions

MSb (M = Ni, Co, Fe, Mn) were obtained by ceramic route syntheses. The electrodes made of the alloys were found to electrochemically react with lithium. The reversible capacity of these materials is of about 320–400 mAh g^{-1}. As for the MnSb electrode the first volumetric discharge capacity is estimated to be 3160 mAh cm^{-3}. XRD results show that MnSb reacted with lithium to form LiMnSb during discharge process. Further lithiation results in the formation of Li_3Sb. During the subsequent charge the reactions are reversible, on fully charge MnSb is regenerated and the presence of LiMnSb phase was observed. The lithium insertion of Li in MnSb alloy has been investigated by ^{121}Sb Mössbauer spectroscopy. During discharge the ^{121}Sb Mössbauer spectra confirm the formation of a new phase "LiMnSb" with the decrease of ferromagnetic MnSb contribution and the coexistence of Li_3Sb. On charge the mechanism is more complex, the formation of MnSb and Li–Sb alloys has been observed. At the end of the charge process the presence of MnSb, LiMnSb alloy and metallic Sb were identified.

Acknowledgements

This work has been supported by SAFT, Bordeaux, France under contract number 752295/00 MP and by ADEME (France).

References

[1] J.-M. Tarascon, M. Armand, Nature, 414 (2001) 15.
[2] H. Huang, E.M. Kelder, J. Schoonman, J. Power Sources 97–98 (2001) 114–117.
[3] H. Li, Q. Wang, L. Shi, L. Chen, X. Huang, Chem. Mater. 14 (2002) 103–108.
[4] J. Yang, M. Winter, J.O. Besenhard, Solid state Ionics 90 (1996) 281.
[5] J.O. Besenhard, J. Yang, M. Winter, J. Power Sources 68 (1997) 87.
[6] R.A. Huggins, J. Power Sources 26 (1989) 109.
[7] R. Alcántara, F.J. Fernandez-Madrigal, P. Lavela, J.L. Tirado, J.C. Jumas, J. Olivier-Fourcade, J. Mater. Chem. 9 (1999) 2517.
[8] J.-M. Tarascon, M. Morcrette, L. Dupont, Y. Chabre, C. Payen, D. Larcher, V. Pralong, J. Electrochem. Soc. 150 (6) (2003) A732.
[9] L. Aldon, A. Garcia, J. Olivier-Fourcade, J.C. Jumas, F.J. Fernandez-Madrigal, P. Lavela, C. Pérez-Vicente, J.L. Tirado, J. Power Sources 119–121 (2003) 585.
[10] H.Z. Dokuzoguz, L.H. Bowen, H.H. Stadelmaier, J. Phys. Chem. Solids 31 (1970) 1565–1571.
[11] A. Onodera, J. Phys. Chem. Solids 60 (1999) 167–179.
[12] T.A. Tumolillo, Phys. Sat. Sol. (a) 17 (1973) 315.
[13] Tu Chen, J.C. Mikkelsen Jr., G.B. Charlan, J. Crystal Growth 43 (1978) 5–12.
[14] N.N. Zhuravlev, G.S. Zhdanov, Ye.M. Smirnova, Phys. Met. Metallogr. 13 (1) (1962) 55–61.
[15] L. Berry, R. Thompson, Mem. Geol. Soc. Am. 85 (1962) 62.
[16] T. Rosenqvist, Acta Metallurgica 761 (1953) 1.
[17] R. Jumar, K.S.H. Vishwamittar, K. Chandra, P. Jernberg, T. Ericsson, R. Wappling, Phys. Rev. Sec. B: Condens. Matter 32 (1) (1985) 69–75.
[18] L.M.L. Fransson, J.T. Vaughey, K. Edström, M.M. Thackeray, J. Electrochem. Soc. 150 (1) (2003) A86–A91.
[19] J.-C. Zheng, J.W. Davenport, Phys. Rev. B 69 (2004) 144415.
[20] J.Z. Li, H. Li, Z.X. Wang, L. Chen, X.J. Huang, J. Power Sources 107 (2002) 1.
[21] S. Grugeon, S. Laruelle, L. Dupont, J.-M. Tarascon, Solid State Sci. 5 (2003) 895.
[22] C.M. Ionica, L. Aldon, P.E. Lippens, F. Morato, J. Olivier-Fourcade, J.-C. Jumas, Hyperfine Interact. 156/157 (2004) 555.
[23] P.E. Lippens, J.-C. Jumas, J. Olivier-Fourcade, Hyperfine Interact. 156/157 (2004) 327.